Form Approved
OBM No. 0704-0188

1. Agency Use Only *(Leave blank).*	2. Report Date.	3. Report Type and Dates Covered.
	20 January 1994	Contractor Report

4. Title and Subtitle.
The Effects of Altimeter Sampling Characteristics: Some Geosat Examples

5. Funding Numbers.

Contract	N00014-92-J-6004
Program Element No.	0601153N
Project No.	3208
Task No.	31-03-4A
Accession No.	DN250131
Work Unit No.	73505603

6. Author(s).
Michael E. Parke* and George Born*

7. Performing Organization Name(s) and Address(es).
*The Regents of The University of Colorado
380 Administrative Center
Boulder, CO 80309-0019

8. Performing Organization Report Number.

9. Sponsoring/Monitoring Agency Name(s) and Address(es).
Naval Research Laboratory
Ocean Technology Branch
Stennis Space Center, MS 39529-5004

10. Sponsoring/Monitoring Agency Report Number.
NRL/CR/7320--93-0004

11. Supplementary Notes.

12a. Distribution/Availability Statement.
Approved for public release; distribution is unlimited.

12b. Distribution Code.

13. Abstract *(Maximum 200 words).*

Altimetric satellites have characteristic sampling patterns in both space and time. This paper looks at the distortions of oceanographic and atmospheric signals as seen in geosat altimeter data. Because of the pattern of ground tracks lain down by Geosat, measurements of oceanographic and atmospheric phenomena can be distorted spatially as well as temporally. As a result, phenomena measured by altimetric measurements can appear as propagating waves with both wavelength and wavenumber different from the original phenomena. These changes, if not understood, can result in misinterpretation of results from altimeter data. Also, in some parts of the world, distorted signals satisfy the dispersion relation of other oceanographic waves, or two phenomena can both have the same distorted dispersion relations. A paper describing the results of this research is in preparation and will be submitted to the Journal of Geophysical Research - Oceans.

14. Subject Terms.
Altimetry, mesoscal oceanography, ocean forecasting

15. Number of Pages.
28

16. Price Code.

17. Security Classification of Report.	18. Security Classification of This Page.	19. Security Classification of Abstract.	20. Limitation of Abstract.
Unclassified	Unclassified	Unclassified	SAR

The Effects of Altimeter Sampling Characteristics: Some Geosat Examples

Final Report to the Naval Research Office
Stennis Space Center, Mississippi

Michael E. Parke
George Born

CCAR, University of Colorado

January 20, 1994

Approved for public release; distribution is unlimited.

Abstract

Altimetric satellites have characteristic sampling patterns in both space and time. This paper looks at the distortions of oceanographic and atmospheric signals as seen in Geosat altimeter data. Because of the pattern of ground tracks lain down by Geosat, measurements of oceanographic and atmospheric phenomena can be distorted spatially as well as temporally. As a result, phenomena measured by altimetric measurements can appear as propagating waves with both wavelength and wavenumber different from the original phenomena. These changes, if not understood, can result in misinterpretation of results from altimeter data. Also, in some parts of the world, distorted signals satisfy the dispersion relation of other oceanographic waves, or two phenomena can both have the same distorted dispersion relations. A paper describing the results of this research is in preparation and will be submitted to the Journal of Geophysical Research - Oceans.

1 Introduction

Despite the phenomenal coverage supplied by altimetric satellites, the measurements of a single satellite are not sufficient to provide a synoptic picture of many atmospheric and oceanographic features. Temporal aliasing (particularly of tides) at a single point has been discussed in other papers (see e.g. Parke et al. 1987, Cartwright and Ray, 1990). In fact, much of the discussion of sampling characteristics has been in terms of temporal aliasing. However, the sampling characteristics of altimetric sampling produce spatial distortions that do not occur in traditional aliasing.

The differences in how an altimetric satellite samples the world occur because the world is not sampled as a snapshot, but rather as a sequence of individual tracks lain down from turning latitude to turning latitude. Thus, in addition to the time between repeats (important for traditional aliasing), the time between adjacent tracks becomes important. This will be discussed more in the following paper. It is important to note, however, that the effects of measuring a given phenomena will be different for different orbit parameters, and in particular can be radically different even for satellites with the same repeat period.

The spatial distortions introduced by altimetric sampling mean that measured phenomena can satisfy different dispersion relations than the underlying phenomena. Because of this, it is possible for some aliased phenomena to satisfy the dispersion relation of other non-aliased oceanographic phenomena or of other aliased phenomena in some parts of the world. Thus, in addition to having aliased phenomena sometimes exhibit unexpected wavelengths, it is possible that in some parts of the world analysis for one type of phenomena will incorporate energy from another type of phenomena, even using knowledge of the dispersion relation.

The purpose of this paper, therefore, is to discuss the spatial as well as temporal characteristics of aliased oceanographic and atmospheric signals, using the Geosat Exact Repeat Mission (ERM) as an example. These results will be used to illustrate some of the possible confusions that can arise and in what parts of the world that the measured dispersion relations of different phenomena coincide.

The following discussion is divided into six sections: the pattern of ground tracks for Geosat, three examples of the effect of sampling generic aliased signals, discussion of the effect of sampling non-aliased signals, discussion of sampling some specific oceanographic signals, examples of the possible confusions between measured phenomena, and a general discussion.

2 Geosat Ground Tracks

ERM ground tracks are lain down in a pattern that is primarily a function of the orbit inclination and the length of the repeat period. The purpose of this section is to describe the time sequence by which independent ground tracks within a repeat period are filled in. On each day, ground tracks will be lain down at evenly spaced intervals (the fundamental interval) toward the west. Ground tracks on successive days will fill in the intervals between the the tracks lain down the first day. For repeating orbits such as the orbit of the ERM, the longitudinal spacing (S) between sequential orbit tracks is equal to the nodal period (P_n) times the difference between the inertial rotation rate of the Earth (ω_E) and the precession rate of the line of nodes ($\dot{\Omega}$);

$$S = P_n(\omega_E - \dot{\Omega}) = \frac{2\pi D}{N} \tag{1}$$

where (N) is the integer number of orbital revolutions and (D) the integer number of nodal days before the ground track repeats. A nodal day is that period between recurrence of the ascending node of the satellite orbit over the same Earth-fixed meridian. Because the precession of the node is much slower than the Earth's rotation rate, a nodal day differs only slightly from a calendar day. All references to repeat days in the rest of this paper will refer implicitly to nodal days. Note that an east positive coordinate system has been adopted, e.g. the nodal precession rate $\dot{\Omega}$ is positive (easterly) for retrograde orbits.

During a repeat period, a complete grid of ground tracks will be produced. The time sequence by which this grid of ground tracks is filled in is determined by the decimal part, q, of the ground track parameter, Q, defined by $Q \equiv N/D = I + q$ where I is an integer and $q < 1$. For repeating orbits, q must be a rational number.

If the fundamental interval is divided into k equal parts (called sub-intervals) where k is the irreducible denominator of q (in this case k represents the repeat period in nodal days), then subsequent tracks within the interval will occur at the sub-intervals with an order determined by the numerator of q. If the numerator is one, then each subsequent track in the interval (at time intervals of approximately one day) will be immediately to the east of the preceding track for both prograde and retrograde orbits. If the numerator is two, then the second track will be two sub-intervals to the east. If it is three, the second track will be three sub-intervals and so forth. Subsequent tracks are filled in in a cyclical fashion.

For the GRM mission, $D = 17$, while $N = 244$. Thus $Q = 14\frac{6}{17}$ and $q = \frac{6}{17}$. This leads to the ground tracks being filled in as in Table I. As can be seen neighboring ground tracks are lain down successively to the east approximately every three days. This pattern is important to the way many sampled phenomena will appear in ERM data. This will be discussed more in the next section.

3 Three Examples of Geosat Sampling

The effect of sampling oceanographic and atmospheric phenomena can be illustrated by looking at three special cases. First suppose that the underlying phenomena is composed solely of a sinusoidal variation in time, but constant phase horizontally, i.e. $h = e^{i\sigma t}$ where h is the amplitude of the underlying phenomena while σ is the angular frequency of the underlying phenomena. This situation corresponds roughly to the aliasing of very broad scale phenomena where the distance between adjacent ground tracks is much less than the wavelength of the measured phenomena. Because the amount of time for a satellite to measure a complete ascending or descending track (~50 minutes for the ERM) is small compared to the time scales of typical oceanographic variations, adjacent ground tracks may be considered to be sampled at a constant time difference apart for purposes of this discussion. Thus if at a given point on a given ground track the underlying phenomena is sampled at times t_j, the equivalent point on the next track to the east will be sampled at times $t_j + \Delta t$. In other words, the measurements at the given point will be $e^{i\sigma t_j}$ while the measurements on the track to the east will be $e^{i\sigma(t_j+\Delta t)}$. If one adopts a local coordinate system aligned with the ground tracks such that y is aligned with the ground tracks while x is normal to the ground tracks, then given a ground track separation of d, the measurements at the adjacent track can be considered as $e^{i\sigma t_j + ik_R x}$ where $k_R = \sigma \Delta t = \frac{2\pi}{\lambda_R}$. Thus, the result of sampling a non-propagating phenomena may be considered as a propagating wave with horizontal wavelength λ_R.

There are then two basic parameters that need to be determined in order to determine the result of sampling a simple signal like this; the change in phase of the underlying phenomena between successive neigboring tracks, $\Delta\kappa_R$, and the change in phase between successive repeat tracks, $\Delta\kappa_T$. Because ground tracks effectively represent the shape of wave crests, the direction of propagation will be at an angle β to the meridion that is normal to the ground tracks, and thus be a function of latitude and whether one is considering ascending or descending ground tracks.

The direction of propagation of the measured wave may be calculated simply by considering that the normal to the ground track is perpendicular to the velocity vector at the measured location. Consider the angle, γ, between a satellite ground track and north (i.e. a meridian) as shown in Figure 1. The angle, γ, is the angle between the meridian and the satellite velocity vector seen by an observer fixed to the Earth. This angle is found by subtracting the Earth's surface rotational velocity vector from the satellite velocity vector projected on the Earth's surface. For a circular orbit the angle, γ, is given by [Parke et al. (1987)] as

$$\gamma = \tan^{-1} abs\left(\frac{V_S \sin\alpha \pm V_E \cos\phi}{V_S \cos\alpha}\right) \tag{2}$$

where the two terms in the numerator are added for retrograde orbits and subtracted for prograde orbits, V_S is the spacecraft velocity

$$V_S = \frac{R_E}{a}\left(\frac{\mu_E}{a}\right)^{\frac{1}{2}} \tag{3}$$

and

$$sin\alpha = abs\left(\frac{cosi}{cos\phi}\right) \tag{4}$$

where i is the inclination of the satellite orbit and phi is latitude. The quantity V_E is the equatorial rotation velocity of the Earth given by $R_E\omega_E$.

The wavelength, λ, of the apparent wave is determined by the distance between ground tracks in the normal direction, and the phase change between adjacent tracks, $\Delta\kappa_R$. The distance between ground tracks, d, is approximately given by

$$d = \frac{S}{17}\sin(\beta) \tag{5}$$

and so the wavelength of the apparent wave is given by

$$\lambda_R = abs\left[\frac{2\pi}{\Delta\kappa_R}d\right] \tag{6}$$

Figure 2 shows the variation in d with latitude. As one follows a ground track towards the turning latitude, the direction of propagation of the apparent wave tends towards north-south, and the wavelength tends towards zero.

The direction of propagation of the apparent wave may be either along the easterly normal or along the westerly normal. This may be determined as follows. Given the east positive coordinate system adopted here, if $\Delta\kappa_R$ and $\Delta\kappa_T$ are of the same sign then the measured phenomena will appear as a westwardly propagating wave. If $\Delta\kappa_R$ and $\Delta\kappa_T$ are of opposite signs then the measured phenomena will appear as an eastwardly propagating wave. These situations are illustrated in Figure 3 using the periods of the M2 and N2 tides.

Second, assume that the underlying phenomena is a plane wave travelling in a crosstrack direction with wavelength λ_U, i.e. $h = e^{ik_U x - \sigma t}$ where $k_U = \frac{2\pi}{\lambda_U}$. When $\lambda_U < 2d$ then the

phenomena will be aliased spatially. For this example, only $\lambda_U > 2d$ will be considered. As before, if at a given point on a ground track the measurements are $e^i k_U x - \sigma t_j$ then the measurements on the adjacent track to the east will be $e^i k_U x - \sigma(t_j + \Delta t)$. These measurements may be considered as $e^{i(k_U + k_R)x - \sigma t_j} = e^{ikx - \sigma t}$ as before. The direction of propagation of the aliased wave will be normal to the ground track with a wavelength given by $\lambda = \frac{2\pi}{k} = \frac{2\pi}{k_U + k_R} = \frac{\lambda_U \lambda_R}{\lambda_U + \lambda_R}$.

The direction of propagation will be determined by the signs of $\Delta\kappa_R + \Delta\kappa_U$ and $\Delta\kappa_T$ where

$$\Delta\kappa_U = 2\pi \left[\frac{d}{\lambda_U}\right] \tag{7}$$

Since $\lim_{\lambda_U \to \infty} \kappa_U = 0$ then $\lim_{\lambda_U \to \infty} \kappa_R + \kappa_U = \kappa_R$ and the limit is case 1 as before. Note that if κ_R and κ_U are of opposite signs, then the direction of propagation will switch as λ_U becomes larger. Figure 4 shows an example of the change in propagation of the measured wave as $lambda_U$ varies. Note that when λ_U and λ_R are equal and of opposite sign, that the apparent wavelength of the measured phenomena is infinite.

Third, assume that the underlying phenomena is a plane wave travelling in an along track direction, i.e. $h = e^{i(l_U y - \sigma t)}$. As before, if the measurements at a point on a given track are $e^{i(l_U y_p - \sigma t_j)}$, then the measurements on the adjacent track to the east will be $e^{i(l_U y_p - \sigma(t_j + \Delta t))} = e^{i(k_R x + l_U y_p - \sigma t_j)}$

In this case, the direction of propagation of the aliased signal will be at an angle, ν, to the ground track given by

$$\nu = tan^{-1} \left[\frac{\lambda_U}{\lambda_R}\right] \tag{8}$$

Note that at the extremes, $lim_{\lambda_U \to 0} \nu = 0$ and $lim_{\lambda_U \to \infty} \nu = \pm\pi/2$. Thus the $lim_{\lambda_U \to \infty}$ represents case 1 as might be expected. As the wavelength of the underlying phenomena trends from zero to infinity, the direction of propagation of the aliased wave rotates from the along track to the cross track direction. Figure 5 shows an example of the change in propagation of the measured phenomena as λ_U varies.

Any plane wave may be considered as being composed of along track and cross track components, and thus its aliased behavior can be discussed in terms of cases 2 and 3 above. An arbitrary wave will have a direction of propagation that rotates to one of the normals to the ground track as λ_U tends to infinity. If one considers a wave for which κ_R and κ_U are of opposite signs, then this rotation will cover an angle greater than 90 degrees. Thus it is

possible for a plane wave with finite wavelength to have an alias that propagates at right angles to the underlying wave.

These considerations will be used to describe the behavior of aliased oceanographic and atmosperic waves in the next sections.

4 Sampling of Unaliased Phenomena

The purpose of this section is to discuss the sampling of unaliased equatorially trapped kelvin waves as an example of the results of sampling unaliased phenomena. Figure 7 shows the dispersion relation of measured unaliased kelvin waves. Note that for a given frequency, the wavelength of the apparent wave is shortened, and that the distortion increases linearly as the frequency increases. It should be noted that the speed of propagation of the measured phenomena will not change, despite the change in slope of the inferred dispersion relation. This is because the inferred dispersion relation has no dynamical significance. However, distortions such as this could lead to problems in interpreting phenomena whose underlying dynamics are not known, even for cases in which the underlying phenomena is not aliased.

5 Some Examples of Sampling Oceanographic Phenomena

It should be noted that the problems of sampling discussed in this paper affect all phenomena that appear in altimeter data, whether oceanographic, atmospheric, related to orbit determination, instrumental, or from other causes. It is the intent of this paper to limit the discussion to oceanographic signals, but similar problems will occur in the analysis of altimeter data due to other sources, such as the effect of sampling atmospheric contributions to the altimeter data. These may well be important in a given analysis.

Because of the complexity of the ocean, its stratification and topography, it would be a daunting task to discuss the result of sampling even all known oceanographic phenomena. It is the intent here to discuss some examples that are either of known importance or thought to be illustrative. The cases chosen here are tides, Rossby waves, and equatorially trapped waves.

5.1 Tides

Tidal variations are pervasive in the deep ocean. Even when the best present solutions are applied to altimeter data, there are still significant residual errors. As discussed below, the result of sampling the tides is a wide variety of frequencies and wavenumbers; often radically different from the original tidal signal.

The temporal aliasing of tides at a single location has been discussed extensively in other publications (see e.g. Parke et al 1987 and Cartwright and Ray, 1990). The purpose here is to investigate the spatial characteristics of these aliases. In regions where the amplitude of a given tidal constituent is locally large, it is often the case that the phase of the tide is slowly varying in space (such locations are often called anti-amphidromes). In these cases, the alias of the tide behaves much like case 1 of section 3. Thus it is meaningful to discuss the sampling of an idealized tide with no spatial variation. Table 2 gives the frequency and wavelength of the alias for the limit λ_U tends to infinity for every tidal constituent for which the equilibrium forcing amplitude is greater than 0.1 cm. Note that the resulting aliased wave can be propagating either along the eastwards normal or the westwards normal. When the apparent wavelength listed in Table 2 is small, the resulting wavelength will appear througout much of the deep water. When the apparent wavelength listed in Table 2 is large, the underlying wavelength of the tide will dominate, and the sampled tide will appear as if it were simply aliased.

It should be noted that techniques for removing orbit error will transfer tidal errors along track. When this occurs, the observed distribution of tidal errors will not match the original distribution of tidal error, but will still show the same imposed sampling pattern. It is the spatial pattern rather than geographic distribution that is the most sensitive indicator of the source of an observed error.

Because the effect of tidal error can become "globalized" in this fashion, the resulting pattern can be mistaken for having another source, such as orbit error.

5.2 Rossby Waves

The apparent frequency and wavenumber of the M2 tidal alias has been shown to satisfy the dispersion relation of first mode baroclinic Rossby waves at mid-latitudes in the Pacific (Jacobs, et al., 1992). It is important to note that the latitude where this occurs is geographically dependent. Figure 8 shows the frequency that barotropic and first mode baroclinic Rossby waves would have to match the wavelength and direction of propagation of the aliased M2 tide. Figure 8 differs slightly from the equivalent figure of Jacobs et al. in that figure 8 uses the internal and external Rossby radii of Emery et al., 1984 for the

longitude 177.5 E while Jacobs et al. uses longitudinally averaged Rossby radii for the entire Pacific basin. Figure 9 shows an equivalent plot to Figure 8, except using the Rossby radii for the cell nearest the European coast in the Atlantic. Note that the latitude where the M2 tidal alias and first mode baroclinic Rossby waves may be confused is now between 18 and 19 degrees north latitude. The more irregular functional form of the curve for first mode baroclinic Rossby waves in the Atlantic is due to the irregular conditions in the nearest cell to the coast in Emery et al.

Figure 10 shows the latitude where the dispersion relation of the aliased M2 tide matches the dispersion relation for a first mode baroclinic Rossby wave as a function of longitude for the North Pacific. Figure 11 shows a similar plot for the North Atlantic. Note the influence of the western gyre in the North Pacific. What this demonstrates is that to fully account for the effects of satellite sampling, one must consider the area being studied and how much local conditions may affect the properties of ocean waves.

5.3 Equatorially Trapped Waves

Two examples will be explored here: Equatorial Kelvin waves and the near 4 day internal gravity wave mode described by for example (Groves and Miyata [1967], Miyata and Groves [1968], Wunsch and Gill [1976]).

Equatorial Kelvin waves can be used as an example of how to use the material presented in this paper to eliminate possible sources of contamination of signals of interest. Equatorial Kelvin waves are characterized by a uniform eastward speed of propagation of about 2.5 m/sec irrespective of wavelength. Thus they may be considered more as travelling blobs than traditional waves. If one calculates the apparent speed of propagation of the aliased tidal constituents as shown in Table 2, then the fastest eastward rate of propagation is about 0.5 m/sec for λ_2 and M1. Since there is a factor of 5 separation between the fastest of the appaent waves due to aliased tides, there should be no problem separating these signals.

For typical equatorial conditions, the near 4 day internal gravity wave mode will be aliased to a frequency of about 4.5 cycles per year and will appear to have a wavelength of about 3.5 tracks. This is very close to the expected appearance of the alias of the Q1 tide as shown in Table 2. In this case, it will be very difficult to separate these signals using only Geosat data.

6 The Consequences of Sampling

There are many ways in which the behavior of sampled phenomena can lead to problems in the interpretation of altimetry data. Most problems can be resolved if the nature of the problem is understood. The examples given in this paper are intended to illustrate the types of problems that can arise.

The simplest problems that arise are those that occur because of mis-identification of patterns. Because many phenomena appear in the altimeter data with both radically different frequency and wavenumber from the underlying phenomena, it is easy to mis-identify them. For example, the M2 and N2 tidal aliases have spatial wavelengths that produce patterns very similar to the patterns created by residual orbit error.

Problems can also occur in situations where the underlying dynamics are not understood. One must be extremely careful in infering the characteristics of the unknown phenomena.

More complicated is the situation illustrated by the M2 tide and first mode baroclinic Rossby waves where the frequency and wavenumber of an aliased phenomena match the dispersion relation of some other oceanographic phenomena. In this case, partial separation of the signals can be obtained by noting that the aliased phenomena will have a different direction of propagaton for ascending and descending tracks, while the unaliased phenomena will appear the same for ascending and descending tracks. Separation will be best at high latitudes where the ascending and descending tracks are perpendicular to one another, and worst near the equator and near the turning latitudes where ascending and descending tracks are most nearly parallel.

The worst situation occurs when the frequency and wavenumber of two aliased phenomena are very close to each other. In this case, separation based on the data at such a location may not be possible. For this situation, more extreme measures need to be taken, such as making solutions for surrounding areas and extending them into the problem region via modelling or other techniques.

7 General Discussion

As has been shown in the preceding sections the signals seen in altimeter data can be radically different than the underlying phenomena that were sampled. Because the nature of the real world signals is dependent on the topography and stratification of the ocean, it is impossible to cover all examples of signals that will create problems in analysis and interpretation. This is especially true in coastal regions where frequencies and wavenumbers are generally higher.

It is hoped that the material presented here will aid in the interpretation of altimeter data by illustrating the nature of problems that can exist, helping attribute strange signals to the correct source, or by eliminating possible sources.

The work presented in this paper is intended to be a foundation for regional studies that can go into more detail about the problems that may exist in a specific area, for studies about the use of data from multiple satellites to aid in the resolution of problem areas, and for planning studies for future satellite missions

Future Work

There are four areas in which this work can be profitably extended

- By investigating the sampling characteristics of the ERS-1 and TOPEX/POSEIDON altimetric satellites
- By investigating the sampling characteristics of orbits not previously chosen for altimetric work
- By investigating the effects of having multiple satellites in either the same orbit or in different orbits
- By investigating the effect of sampling characteristics on errors in non-oceanographic signals in the altimeter data, such as errors in the estimates of the dry tropospheric contribution.

This last will be of importance to oceanographic studies, since it is in principle possible for atmospheric signals to appear to have some or all of the characteristics of oceanographic signals even when the underlying atmospheric phenomena don't.

References

Cartwright, D.E. and R.D. Ray, Oceanic tides from Geosat altimetry, *J. Geophys. Res.* , **95 (C3)** , 3069-3090, 1990.

Emery, W.J., W.G. Lee, and L. Magaard, Geographic and seasonal distributions of Brunt-Vaisala frequency and Rossby radii in the North Pacific and North Atlantic, *JPO* , **14** , 294-317, 1984.

Groves, G.W. and M. Miyata, On weather-induced long waves in the equatorial Pacific, *J. Mar. Res.* , **24** , 115-128, 1967.

Jacobs, G.A., An analysis of rossby waves in the Pacific ocean from Geosat altimetry data, PhD Thesis, University of Colorado, Boulder, Colorado, 163pp, 1991.

Miyata, [illegible] and G.W. Groves, Note on sea-level observations at two nearby stations, *JGR* , **73** , 3965-3967, 1968.

Parke, M.E., R.H. Stewart, D.L. Farless and D.E. Cartwright, On the choice of orbits for an altimetric satellite to study ocean circulation and tides, *J. Geophys. Res.* , **92 (C11)** , 11693-11707, 1987.

Wunsch, C. and A.E. Gill, Observations of equatorially trapped waves in Pacific sea-level variations, *Deep Sea Res.* , **23** , 371-390, 1976.

Table 1: Order of ground tracks for the GRM mission. On day zero, the track at the far right will be lain down, followed approximately 100 minutes later by the track at the far left. Approximately one day later the track marked 1 will be filled in followed on day two by the track marked 2 and so on. On day seventeen, the track at the far right will be repeated followed by the track at the far left. East is to the right.

0	3	6	9	12	15	1	4	7	10	13	16	2	5	8	11	14	0

Table 2: Alias Frequency and Wavelength for Selected Tidal Constituents (with maximum equilibrium amplitude exceeding 0.1 cm)

Equilibrium Amplitude	Period (hrs)	Symbol	Frequency (cpy)	Equatorial Wavelength
Terdiurnal Tide				
0.22	8.2804008	M3	8.98	3.44
Semidiurnal Tides				
16.83	12.4206012	M2	1.15	-5.16
7.83	12.0000000	S2	2.16	-104.2
3.26	12.6583482	N2	7.01	3.30
2.13	11.9672348	K2	4.16	-38.39
0.63	12.6260044	$\nu 2$	8.79	3.47
0.47	12.1916202	L2	9.32	-11.78
0.46	12.0164492	T2	1.16	-732.0
0.44	12.9053745	2N2	6.24	-2.43
0.41	12.6604146	-	6.90	3.29
0.41	12.8717576	$\mu 2$	4.47	-2.52
0.39	12.1897040	-	9.21	-11.91
0.12	12.2217742	$\lambda 2$	10.33	10.06
0.12	11.7545217	KJ2	4.00	7.40
0.11	12.9075223	-	6.36	-2.42
Diurnal Tides				
9.83	23.9344697	K1	2.08	-76.79
6.99	25.8193417	O1	3.23	-4.83
3.25	24.0658902	P1	0.08	291.5
1.35	26.8683567	Q1	4.93	3.16
0.59	24.8332484	M1	10.25	10.41
0.55	23.0984768	J1	6.08	8.19
0.30	22.3060742	OO1	7.40	-4.29
0.26	26.7230533	$\rho 1$	6.71	3.32
0.25	23.0915993	-	5.97	8.13
0.21	26.8776683	-	4.82	3.16
0.19	24.1321400	$\pi 1$	0.92	-85.78
0.18	28.0062225	2Q1	8.32	-2.35
0.14	23.8044765	$\phi 1$	4.08	-33.92
0.11	27.8483876	$\sigma 1$	6.55	-2.44
0.11	25.8107490	-	3.12	-4.85
Long Period Tides				
2.90	327.858969	Mf	5.32	-4.55
1.53	661.309205	Mm	8.17	9.17
1.35	4382.90521	Ssa	2.00	-60.78
0.74	655.717998	-	8.05	9.09
0.56	219.190386	-	2.85	3.04

Figure Captions

Figure 1: Ground track geometry after Parke, et. al, 1987

Figure 2: Ground track spacing as a function of latitude

Figure 3: Sampling of a spatially uniform idealized M2 tide. Each solid line represents the measured tide at one of six equally spaced times during the aliased tidal cycle (1.15 cycles/year). Successive measurements of the idealized tide have been offset vertically by one meter. Note the apparent westward propagation of the measured tide.

Figure 4: The same as figure 3, except for N2 (aliased frequency 7.01 cycles/year). Note the apparent eastward propagation of the measured tide.

Figure 5: Apparent wavelength of a measured plane wave travelling in a cross track direction as a function of the wavelength of the underlying wave. Note that when the wavelength of the underlying wave is small, the underlying wave dominates the wavelength of the apparent wave, while when the wavelength of the underlying wave is large, the sampling of the satellite dominates.

Figure 6: The apparent wavelength and direction of propagation of the apparent wavelength of a measured plane wave travelling in an along track direction as a function of the wavelength of the underlying wave. Each point on the displayed curve represents the results of sampling one underlying wavelenth. If a vector is drawn from the origin to a point on the displayed curve, then the angle from the vertical axis represents the angle of propagation of the measured wave with respect to the along track direction while the length of the vector represents the wavelength of the apparent wave. The left end of the curve represents the case where the underlying wavelength tends to zero, while the right end of the curve represents the case where the underlying wavelength tends to infinity. Note that when the underlying wavelength tends to be small, the propagation of the apparent wave tends to be along track, while when the underlying wavelength tends to be large the propagation tends to be cross track.

Figure 7: The apparent dispersion relation of unaliased equatorial kelvin waves. Note that for the underlying kelvin wave $\hat{\kappa} = \hat{\omega}$. Thus the effect of the geosat sampling is to stretch the wavelength of the underlying wave with the percentage amount of stretch increasing linearly as the frequency of the underlying wave increases.

Figure 8: The frequency of barotropic (top curve) and first mode baroclinic Rossby waves with the same wavelength and direction of propagation as the M2 tidal alias. The horizontal line is the aliased frequency of the M2 tide. The curves are base on the internal and external

Rossby radii of deformation for 177.5 E after Emery et al, 1984.

Figure 9: The same as Figure 8, except for the cells nearest the European coast in the North Atlantic.

Figure 10: The latitude at which the aliased M2 tide satisfies the dispersion relation of a first mode baroclinic Rossby wave as a function of longitude for the North Pacific.

Figure 11: The same as Figure 10, except for the North Atlantic.

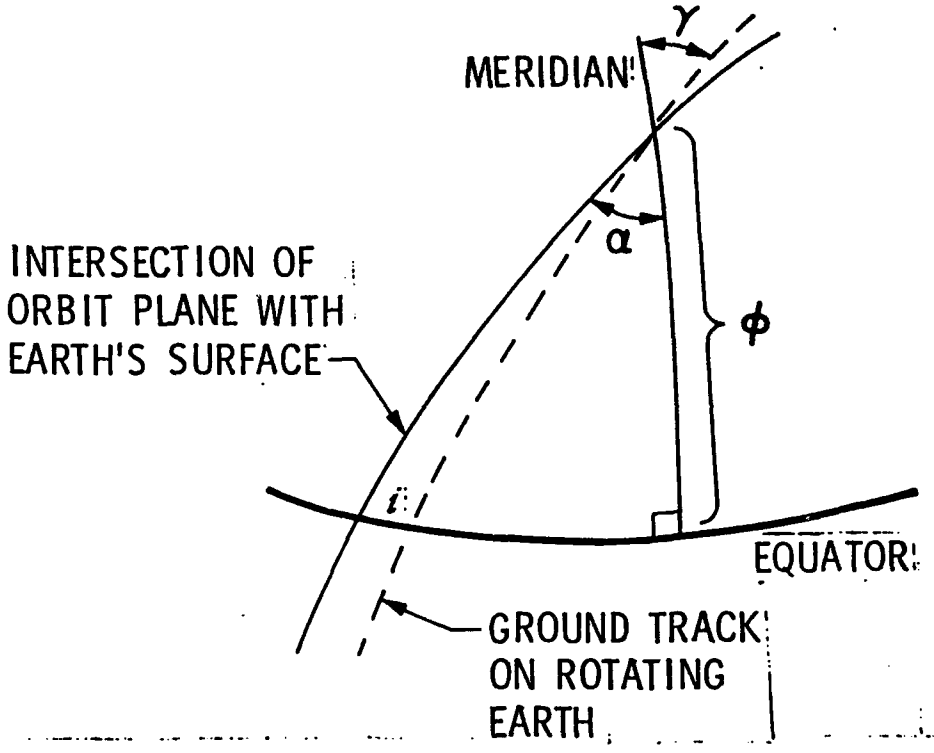
MERIDIAN
γ
α
ϕ
INTERSECTION OF
ORBIT PLANE WITH
EARTH'S SURFACE
i
EQUATOR
GROUND TRACK
ON ROTATING
EARTH

Fig 1

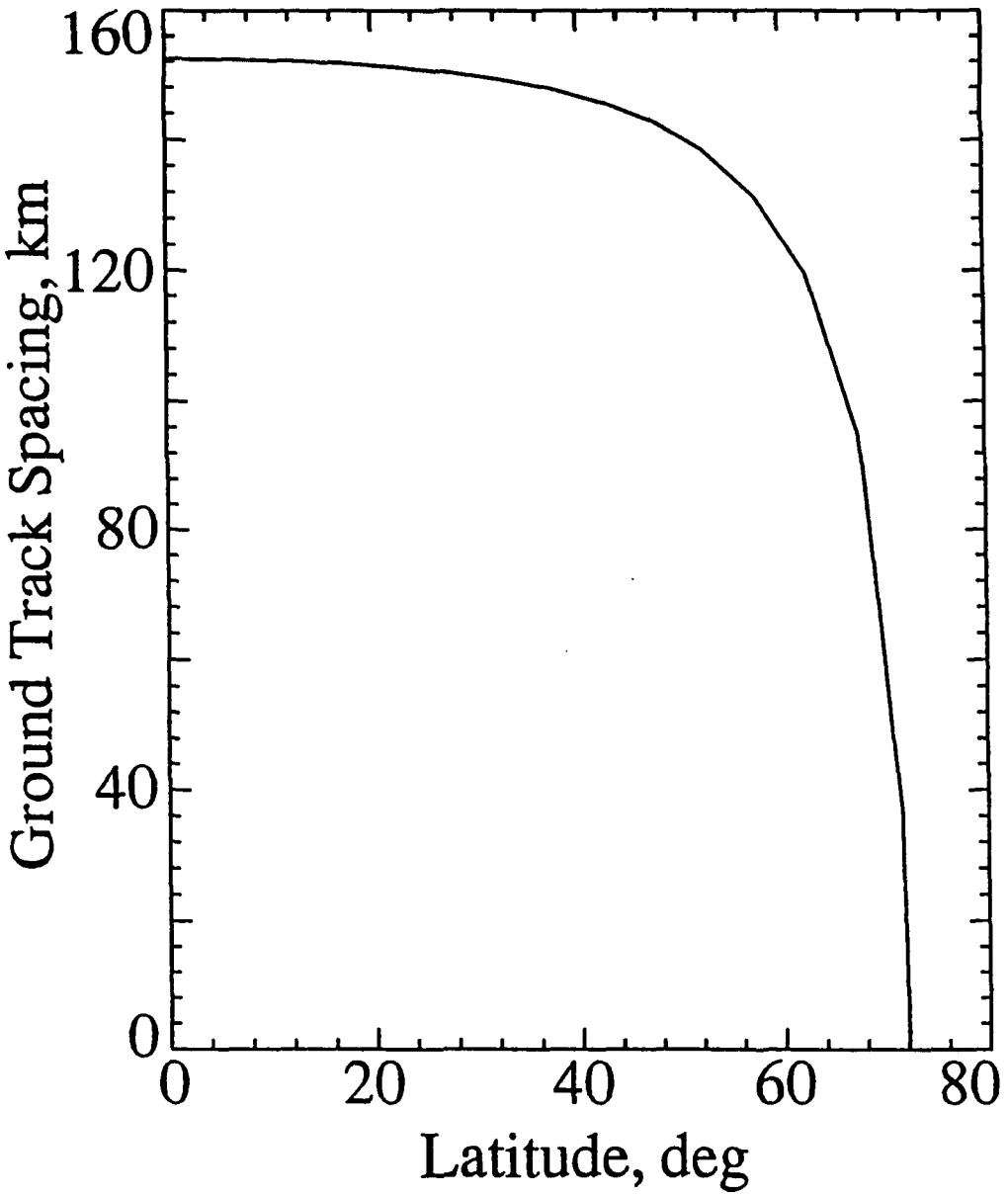
160
120
80
40
0
Ground Track Spacing, km
0
20
40
60
80
Latitude, deg

Fig 2

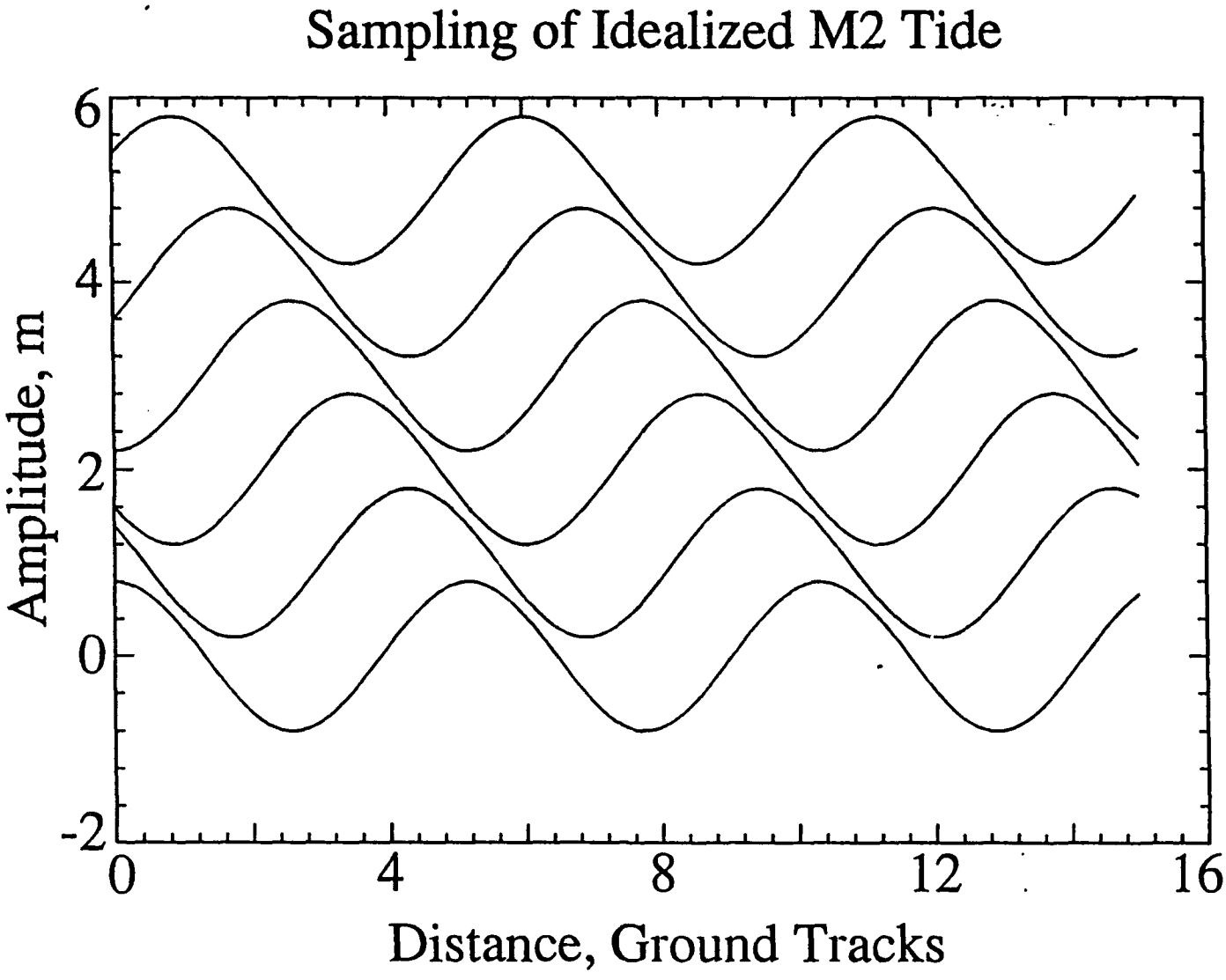
Sampling of Idealized M2 Tide
Amplitude, m
6
4
2
0
-2
0
4
8
12
16
Distance, Ground Tracks

Fig 3

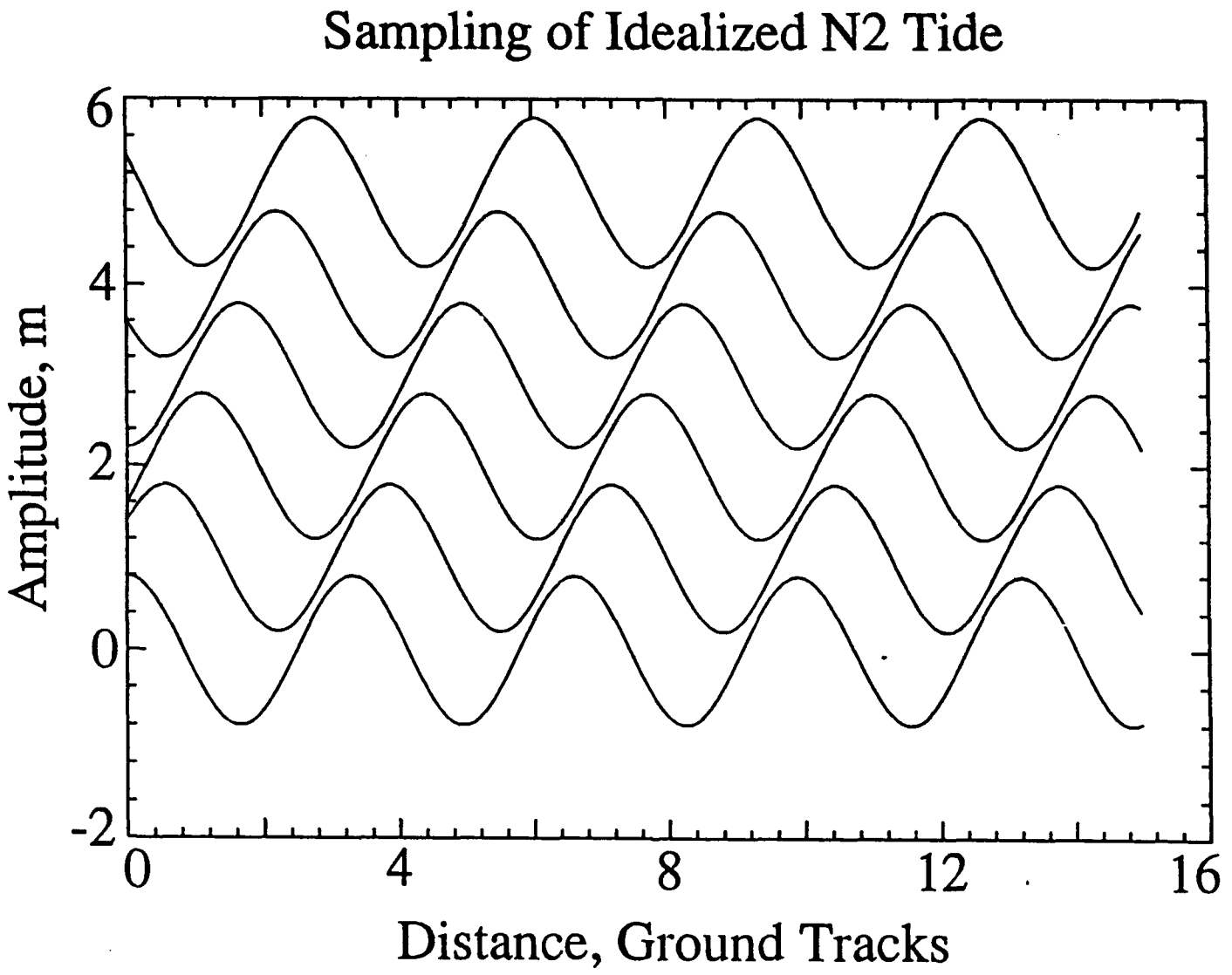
Sampling of Idealized N2 Tide
Amplitude, m
6
4
2
0
-2
0
4
8
12
16
Distance, Ground Tracks

Fig 4

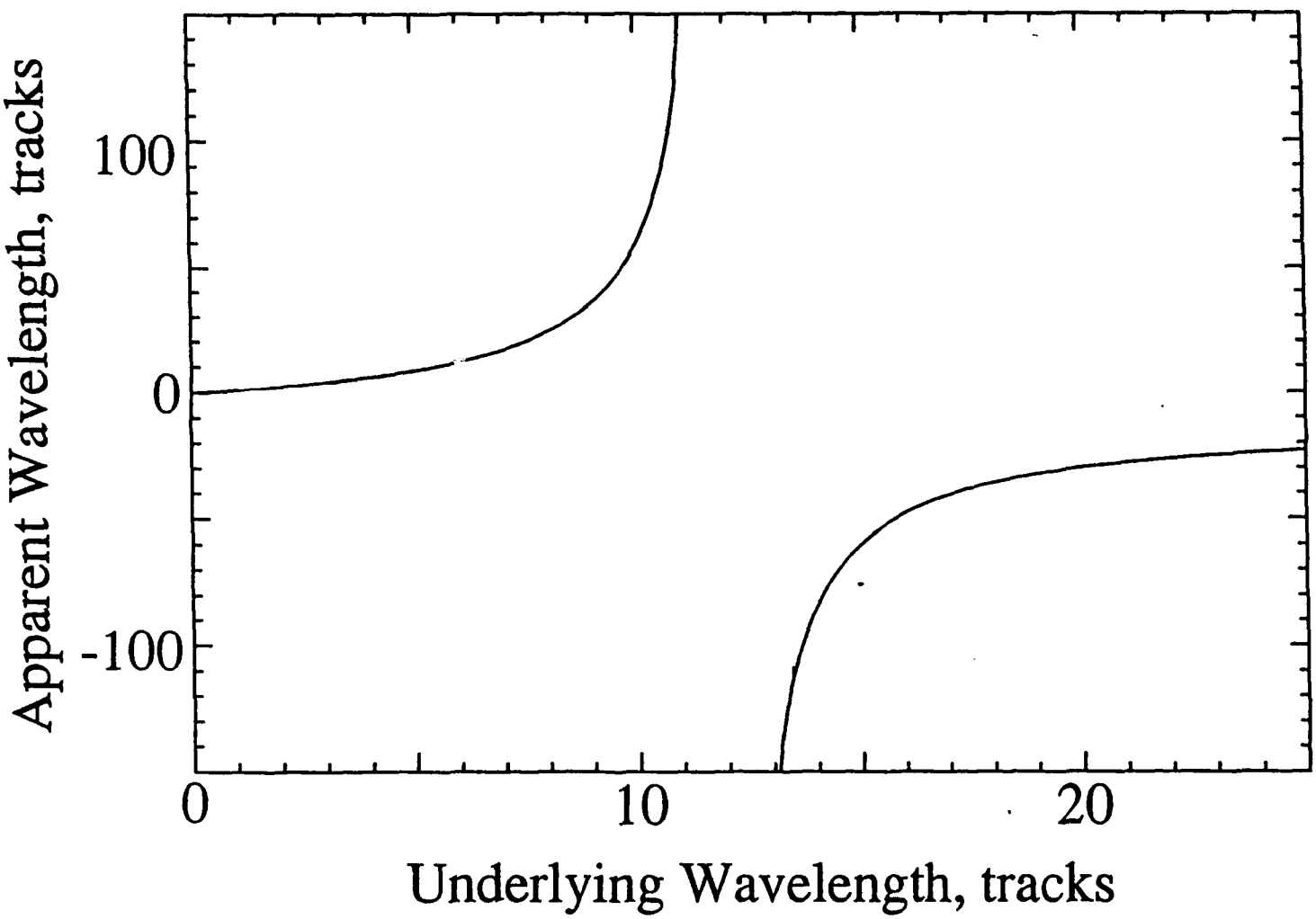
Apparent Wavelength, tracks
100
0
-100
0
10
20
Underlying Wavelength, tracks

Fig 5

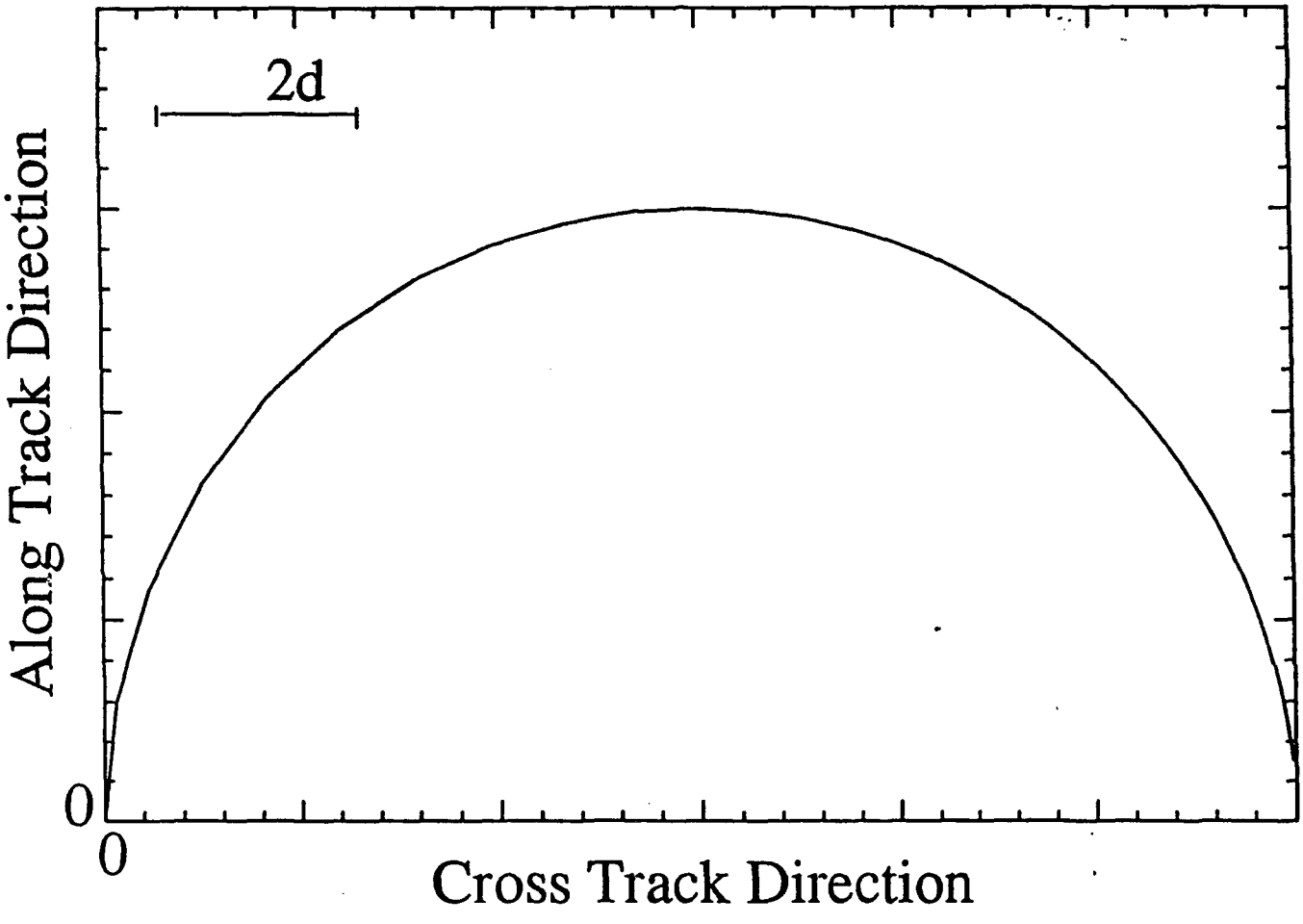

Fig 6

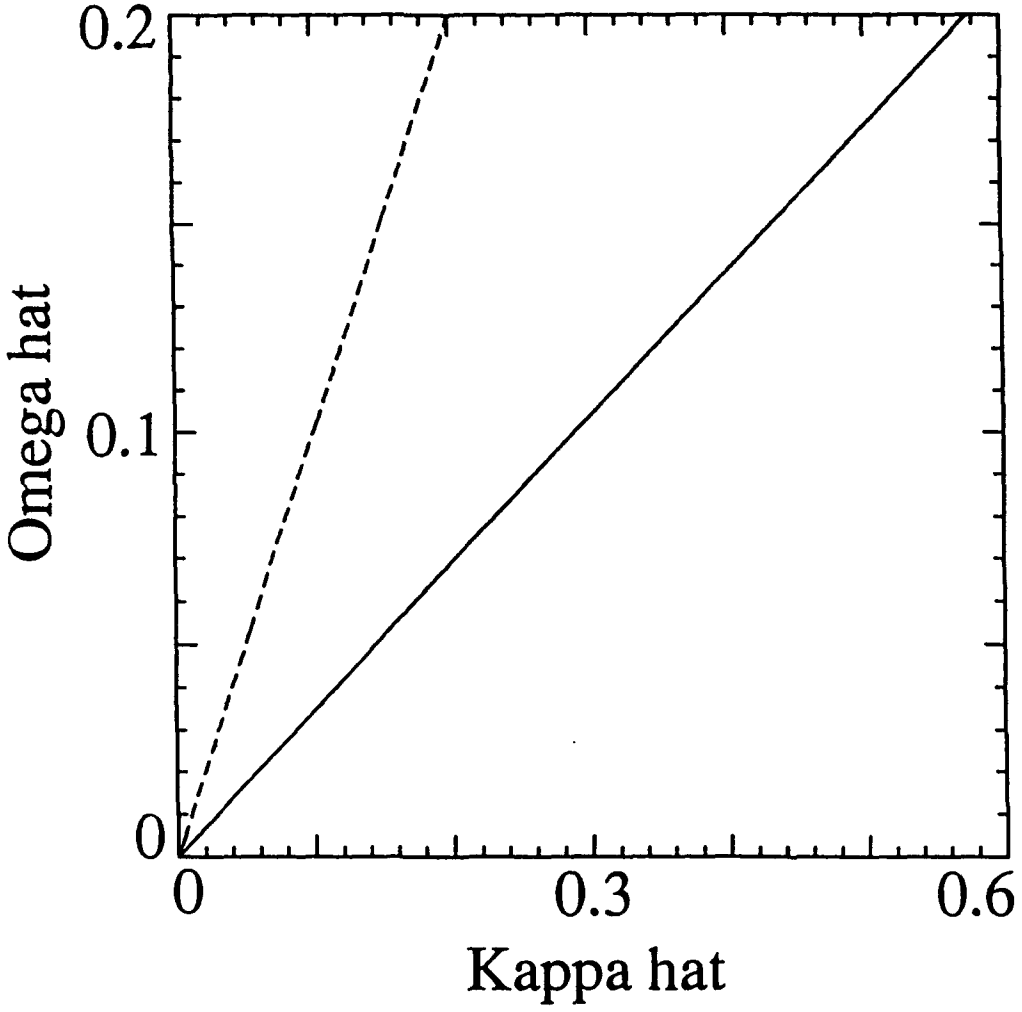

Fig 7

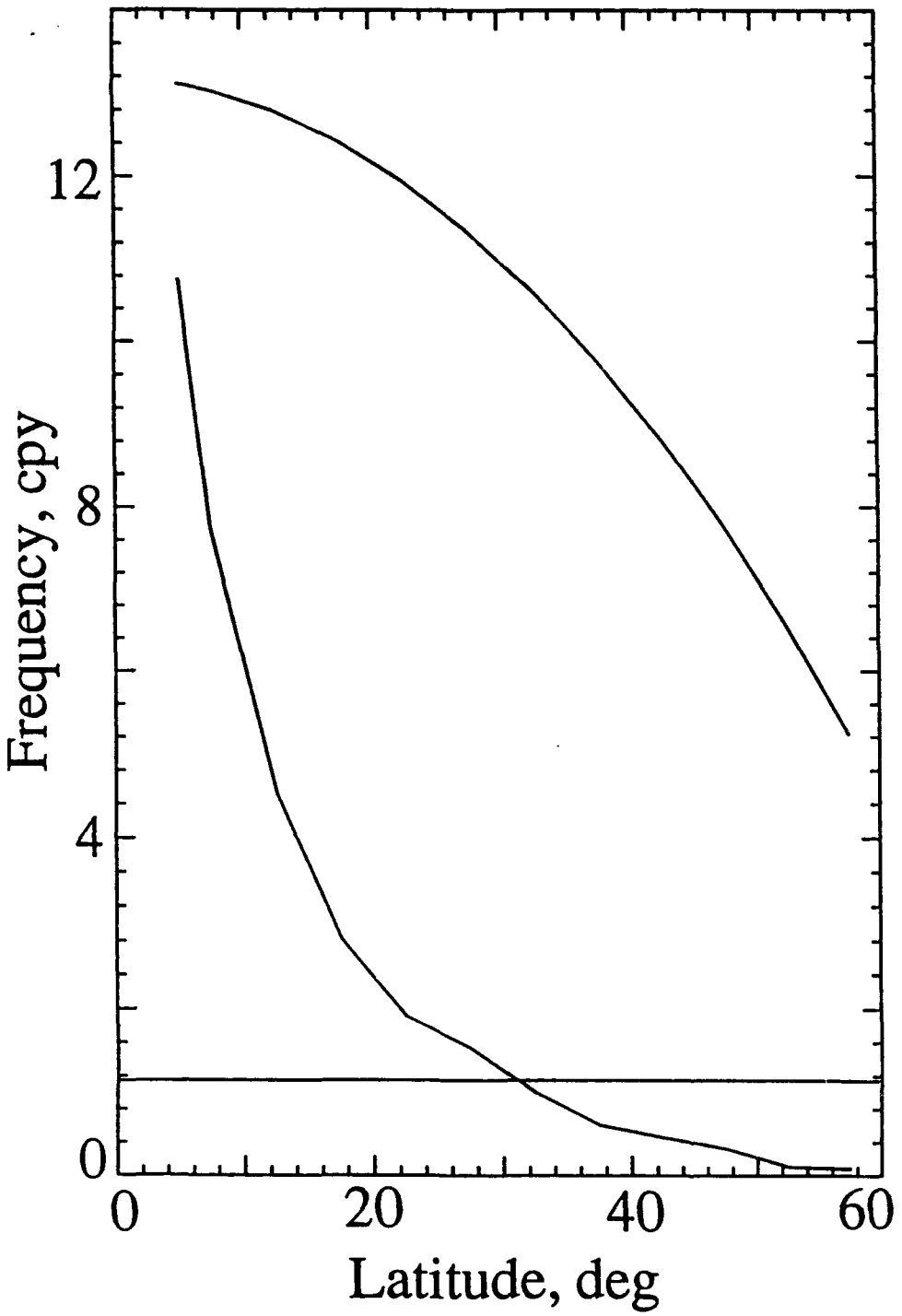

Fig 8

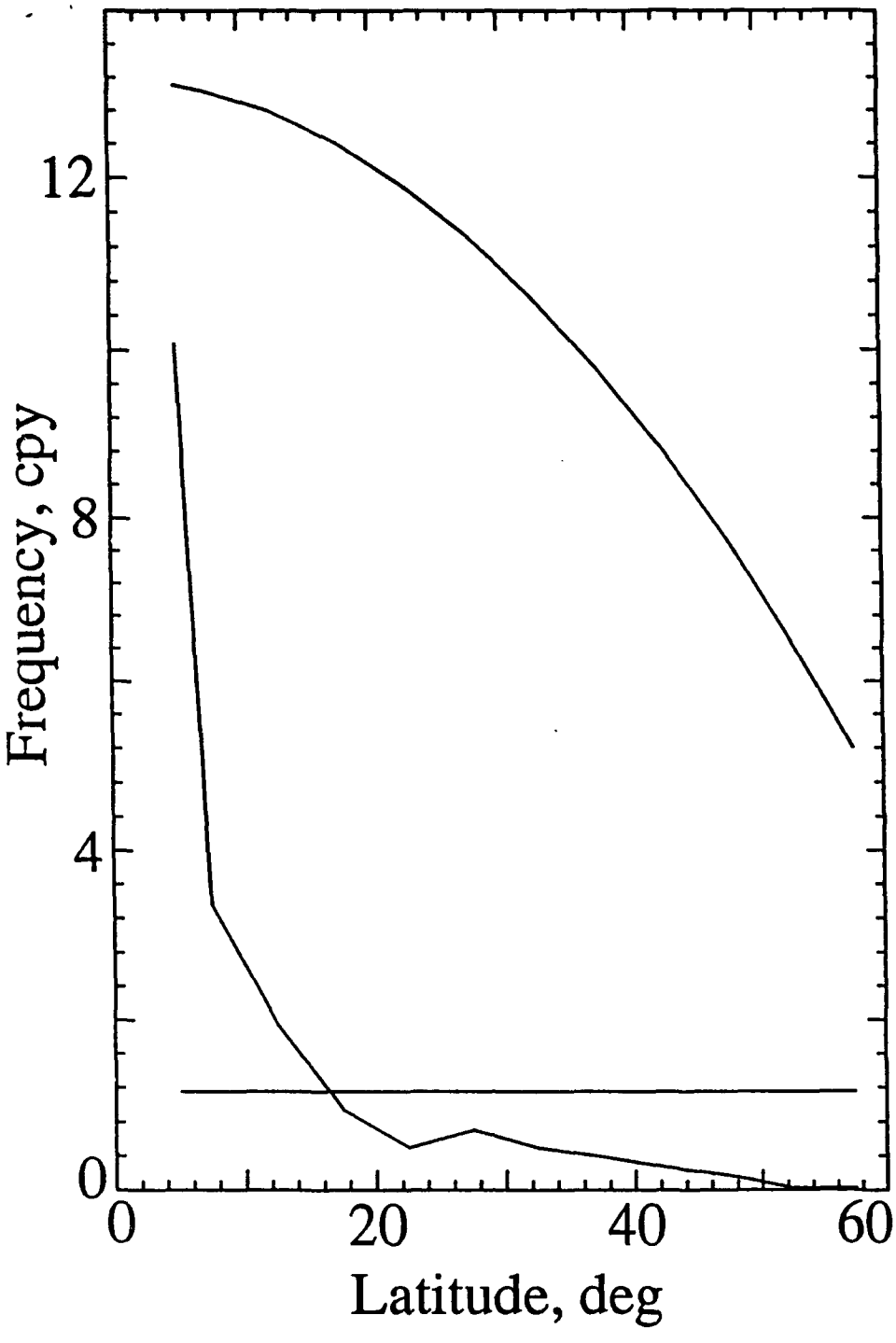

Fig 9

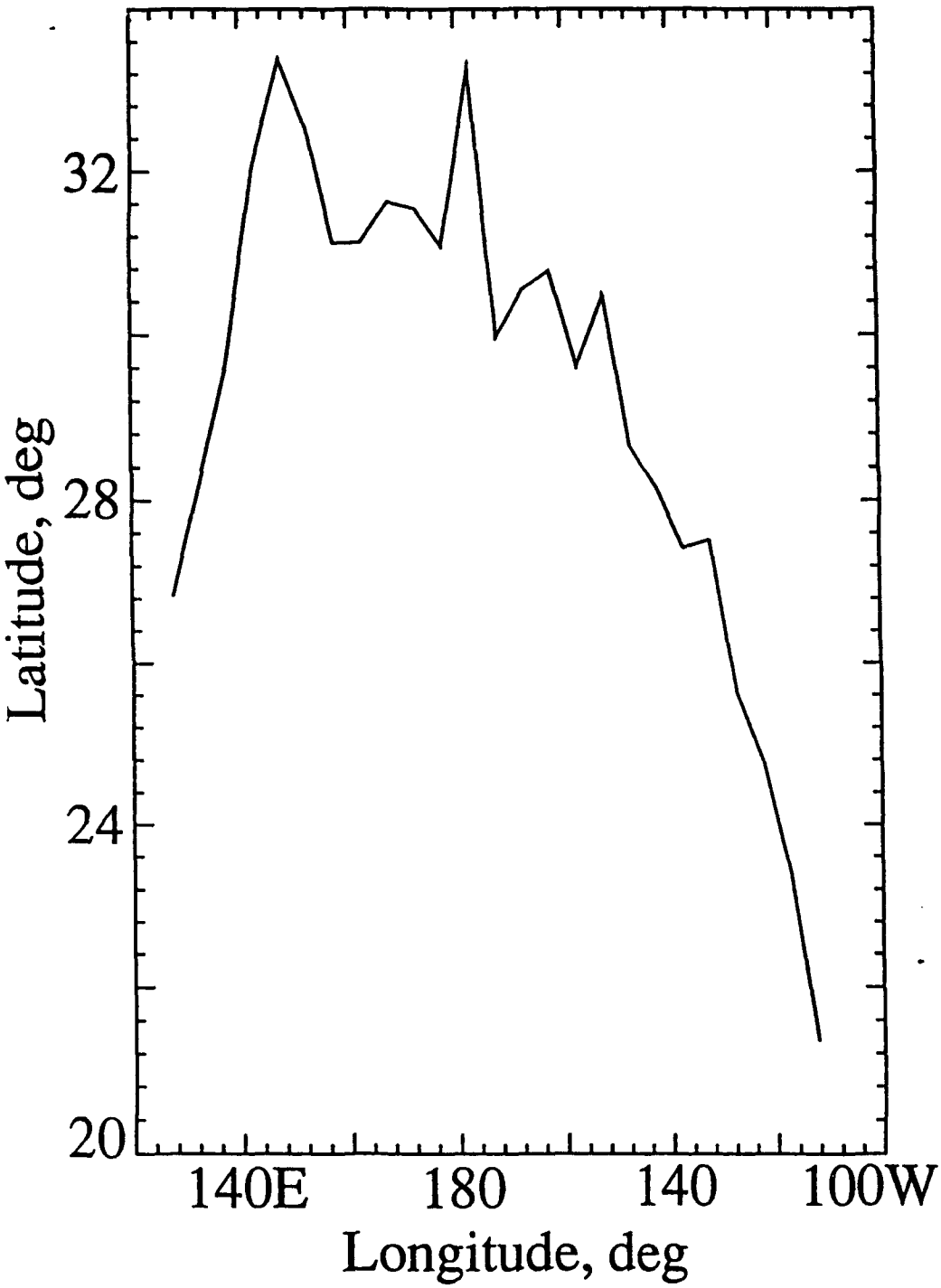

Fig 10

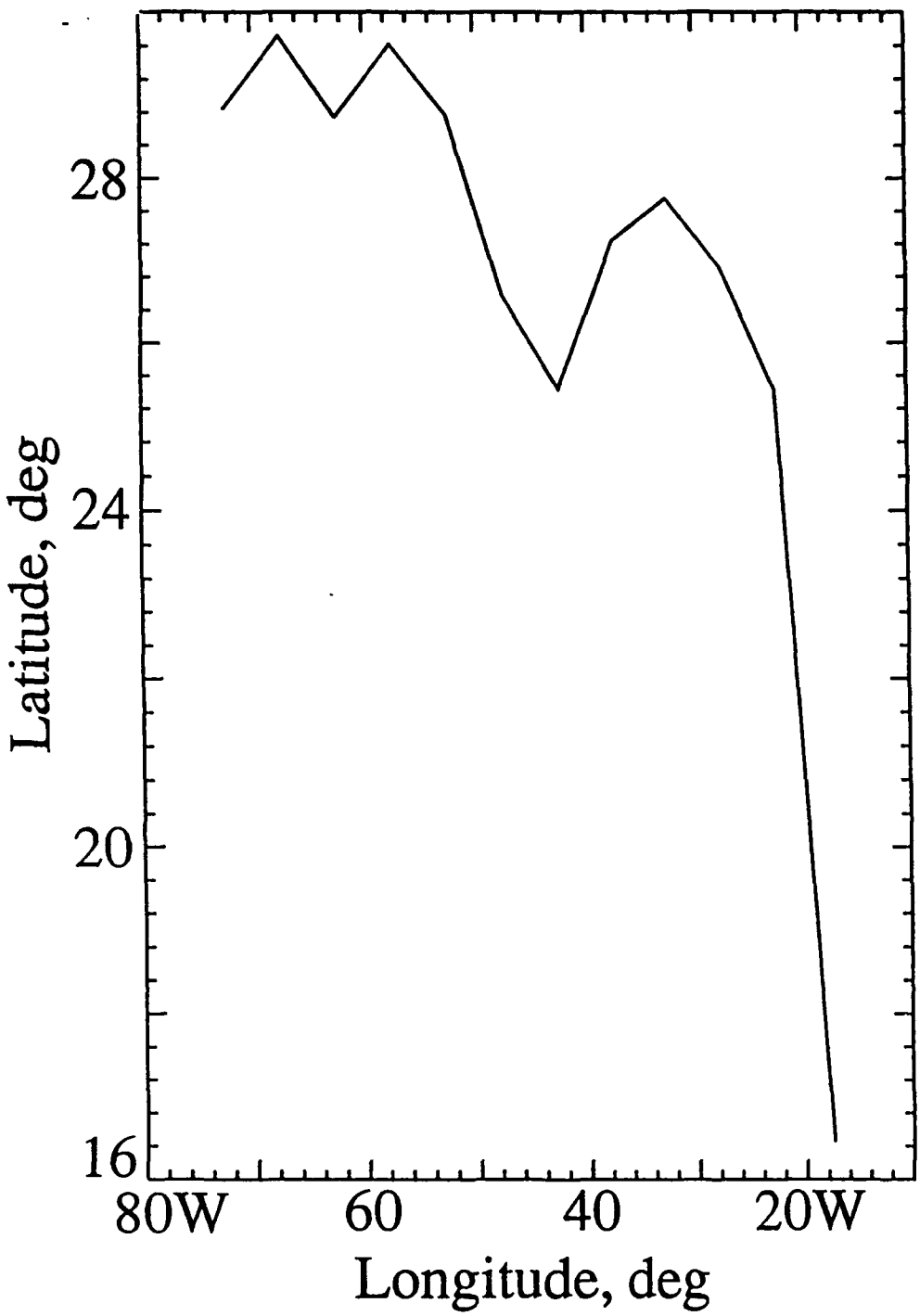

Fig 11